SLOPE

SLOPE STABILITY ANALYSIS TOOL

Verification of the Slope Limit-Equilibrium Engine

Against Published Benchmarks

hetGE · v0.10.0 · 2026-07-23

Tolga Y. Ozudogru

DRAFT, FOR INTERNAL REVIEW

Contents

Abstract 3

1. Introduction 3

2. Verification methodology 6

2.1 Sources 6

2.2 Protocol 6

2.3 Independence checks 7

3. Results 8

3.1 SLOPE/W (ACADS) suite 8

3.2 Slide2 suite 12

3.3 Reinforcement 15

4. Discussion 16

4.1 Method-specific observations 16

4.2 Janbu correction 17

4.3 A discrepant published case 17

4.4 Scope exclusions 17

5. Limitations 18

6. Conclusions 18

References 19

Appendix A: Replicated Slide2 models and results 20

Table A1: Model configurations 20

Table A2: Factor-of-safety comparison 22

Abstract

We present a systematic verification of the slope-stability calculation engine used in *Slope* (hetGE) against two independent, published verification suites: the GeoStudio **SLOPE/W 2D Verification Manual** and the Rocscience **Slide2 Slope Stability Verification Manual** (111 problems, © 2022 Rocscience Inc.). Every applicable problem was rebuilt from the manuals' tabulated inputs and solved with the engine's limit-equilibrium methods: Ordinary (Fellenius), simplified Bishop, simplified Janbu with the f_0 depth correction, Spencer, and a full Morgenstern–Price (GLE) implementation, with Corps of Engineers and Lowe–Karafiath as consistency-verified force-equilibrium variants, using the engine's automatic critical-circle search, its weak-layer **block search**, or, where the source specified one, the exact published slip surface, circular or **non-circular (polyline)**. Across **61 replicated cases** (8 SLOPE/W + 53 Slide2), spanning layered profiles, phreatic and r_u pore pressure, pseudo-static seismic loading, dry and water-filled **tension cracks**, a **reinforced (micro-pile) slope**, **non-circular slip surfaces** (a predefined weak-seam polyline, two block searches, and a composite circular surface reconstructed along a weak layer), **depth-varying undrained strength**, **uniform and linearly-varying (trapezoidal) surcharges**, and imperial and metric units, the simplified-Bishop factor of safety agrees with the published values with a **mean absolute deviation of 1.0 % (median 0.8 %, maximum 4.7 %)**, the Morgenstern–Price factors agree with published GLE/Spencer values with a mean deviation of 1.7 %, and the Spencer factors agree with the manuals' published Spencer values with a mean deviation of 1.9 % across 43 cases. 57 of the 59 primary comparisons fall within 5 %; the two exceptions are both search-landscape divergences on the same dipping ACADS weak-layer mechanism. The first is the Slide2 block-search case #7 (−5.9 %), where the engine's search converges to a different (more critical, conservative-side) block than the manual's own, corroborated by the GeoStudio variant of the identical problem (−4.8 %) and refuted as a solver defect by the specified-surface companions (−0.6 %). The second is the SLOPE/W §2.9 external-loading case (+6.7 %), the family's fourth member, which layers a piezometric surface and a new linearly-varying (trapezoidal) surcharge onto the same dipping seam: here GeoStudio's manual restricted its own search to circular surfaces, while the seam's true critical mechanism is non-circular, so our block search finds it and matches the identical problem's Slide2 publication (its own block-searched GLE value) to +2.1 % (Slide2 #9). The largest Bishop deviation (4.7 %) is the depth-varying-undrained-strength case #23, on which the published sources themselves span 1.14–1.19 (our value matches Low's original 1.14 to 0.4 %); the next largest (4.2 %) is the ACADS tension-crack case, on which the two commercial manuals themselves disagree by 4.1 % (our value matches Slide2's to 0.5 %). The one published **reinforced** benchmark, Slide2 #54's single-row of stabilising micro-piles, is reproduced to +1.4 % (Bishop 1.209 vs published 1.193), and the engine's four reinforcement element types (anchor, soil nail, geosynthetic, pile) are demonstrated on a common slope. One published case (#44a) was found to be internally inconsistent with its own stated inputs, confirmed by an independent hand calculation. Problems outside the engine's scope (73 of 111 in the Slide2 suite) are catalogued with per-problem reasons.

1. Introduction

Slope computes the stability of two-dimensional soil slopes by the method of slices on circular and **non-circular (polyline)** slip surfaces. The calculation engine is a pure, headless TypeScript module, independent of the user interface, which makes it directly scriptable for verification camp-

aigns like the one reported here.

The engine implements:

- **Methods.** Ordinary (Fellenius), simplified Bishop (moment equilibrium, iterated), simplified Janbu (force equilibrium, iterated) with the Janbu f_0 depth correction, and **Morgenstern–Price**, a full general-limit-equilibrium (GLE) formulation with a half-sine interslice force function, in which the moment factor F_m and force factor F_f are iterated with the interslice force profile refreshed each pass, and the interslice scale λ is driven until $F_m = F_f$ by a pole-aware bracketed search. **Spencer** is solved on the same GLE chassis with a constant interslice function $f \equiv 1$ (interslice inclination $\theta = \arctan\lambda$); **Corps of Engineers** (interslice inclination fixed at the daylight-chord slope) and **Lowe–Karafiath** (per-boundary average of the ground and slip-surface inclinations) run the same co-iteration with $\lambda = 1$ and report the force-equilibrium factor F_f. Interslice shear is zero at both end boundaries for the whole GLE family.
- **Slicing.** Vertical slices whose edges are break-aligned to the ground polyline (no slice straddles a slope break), with column integration of weight, centroid and base properties per slice.
- **Search.** Two automatic parameterizations of the critical circle: a center-grid × radius-fan sweep with local refinement, and a GeoSlope-style **entry–exit** sweep of daylight points (with user-restrictable entry/exit ranges, used in this study to reproduce a benchmark's "focus object" search). Impenetrable (bedrock) regions act as keep-outs; a minimum-depth filter rejects skin slips.
- **Non-circular surfaces.** Fully-specified **polyline** slip surfaces (drawn in the app or taken verbatim from a benchmark table) are analyzed directly, and a targeted **block search** for weak-layer mechanisms samples two rectangular windows bracketing the seam and projects active/passive wedge fans ($45^\circ \pm \varphi/2$, swept $\pm 12^\circ$) up to the ground surface at each end, with local refinement about the best block. Bishop and Ordinary presume the common-center moment arm and are gated to circular surfaces; the GLE family and Janbu run on polylines.
- **Strength models.** Mohr–Coulomb; undrained ($\varphi = 0$) with constant or **linearly depth-varying** c_u (gradient off the layer top, optional cutoff) and SHANSEP stress-history strength; Generalized **Hoek–Brown** (local-tangent equivalent Mohr–Coulomb at the slice's σ'_n); hyperbolic; two-set anisotropic; and no-strength / impenetrable regions.
- **Pore pressure.** Dry, a phreatic/piezometric line (hydrostatic below the line, $u = \gamma_w h$), or a constant pore-pressure coefficient r_u; the water unit weight is configurable, so imperial-unit problems run natively.
- **Probabilistic analysis.** A seeded Monte-Carlo / Latin-hypercube layer samples material parameters (γ, c, φ / c_u) and the seismic coefficient about the deterministic model, with optional c–φ correlation, and reports the probability of failure and reliability index β (normal and log-normal). None of the manuals' probabilistic problems is extractable from tabulated inputs (§4.4), so this layer sits outside the FoS-accuracy study below.
- **Actions.** Pseudo-static seismic coefficients k_h and k_v, with the *critical horizontal direction determined automatically* (both shaking directions are solved and the lower factor governs); uniform or linearly-varying (trapezoidal) surcharges and vertical line loads on the ground surface; reinforcement elements (anchors, nails, geosynthetics, piles) resolved at the slip-surface crossing.
- **Tension cracks.** A crack-bottom polyline defines the cracked zone: every trial surface is truncated with a **vertical crack face** where it crosses the line on the crest side (the truncated

soil carries neither strength nor weight), and a (partially) water-filled crack pushes the mass with the hydrostatic thrust $\frac{1}{2}\gamma_w z_w^2$ acting at $z_w/3$ above the crack bottom, entering the moment methods through its moment about the circle center, the force methods through the horizontal force balance, and the M-P interslice recursion through its E-boundary closure.

- **Design standards.** Seventeen built-in partial-factor sets across seven code families: Eurocode 7 (EN 1997-1:2004 Design Approaches 1·C1, 1·C2, 2, 3, and the second-generation EN 1997:2024 VC3+M2), **AASHTO LRFD** (2024 Strength I and Extreme Event I), **BS 8006** (1995/2010), **AS 4678** (2008) and **CSA S6:19** (CHBDC), plus fully custom sets. Every factor is applied *inside* the solver (materials, soil weight, actions, reinforcement and seismic each factored at the slice, never a post-solve divisor).
- **Units.** Each model carries a unit system: SI (kN, kPa, m) or US customary (lb, psf, ft). The engine computes in consistent units with a configurable unit weight of water, so results are unit-invariant and imperial-unit problems run natively.

All computations in the FoS-accuracy study below used the plain factor-of-safety set (all partial factors = 1); the partial-factor machinery is verified separately, each set unit-tested to its exact factoring ratio (e.g. Eurocode 7 DA2 lowers the factor of safety by precisely 1/1.1, and DA1·C2 divides $\tan\varphi'$ and c' by 1.25).

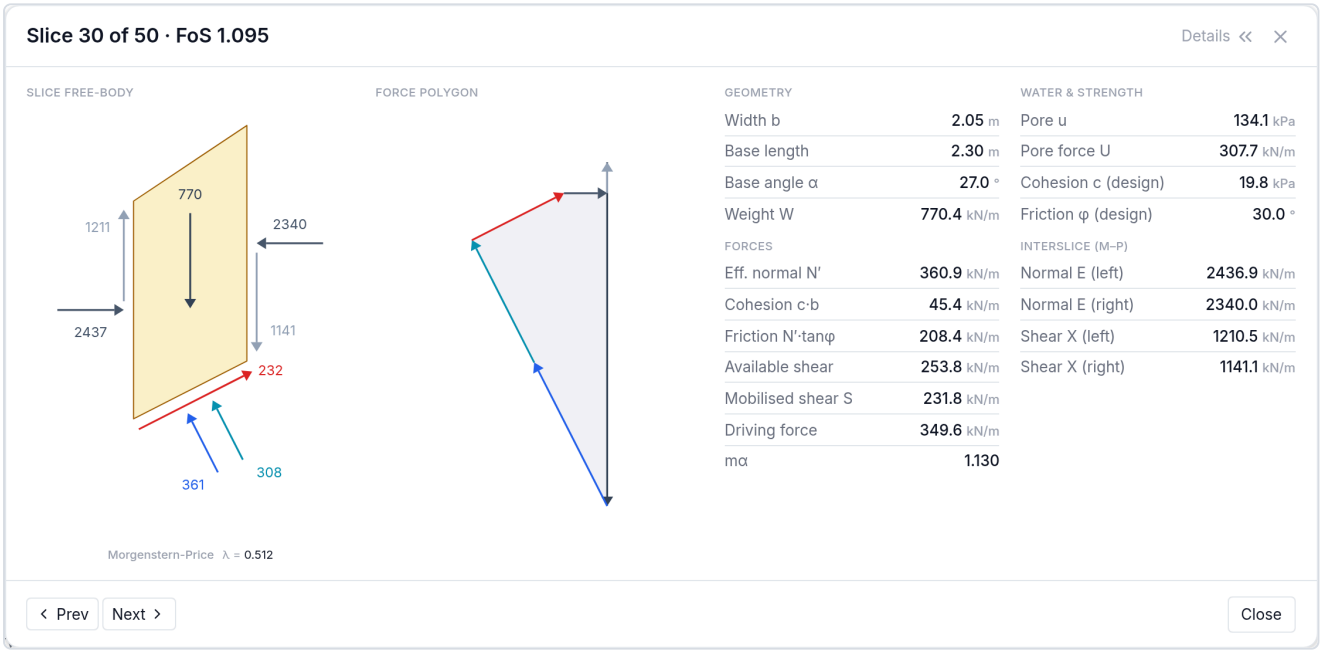


Figure 1. The application's slice inspector on a solved Morgenstern–Price surface (slice 30 of 50, Slide2 #20). Each slice exposes its **free body** (left), carrying weight W, base effective normal N', pore force U, mobilised shear S and the Morgenstern–Price interslice normals E and shears X on the slice faces, together with the tip-to-tail **force polygon** (right), which closes for the rigorous solution: a direct visual check that the slice is in force equilibrium. The side panels list the geometry, pore pressure, strength, per-slice force breakdown and interslice values entering the equations, with the Bishop m_α term and the solved interslice-force inclination λ.

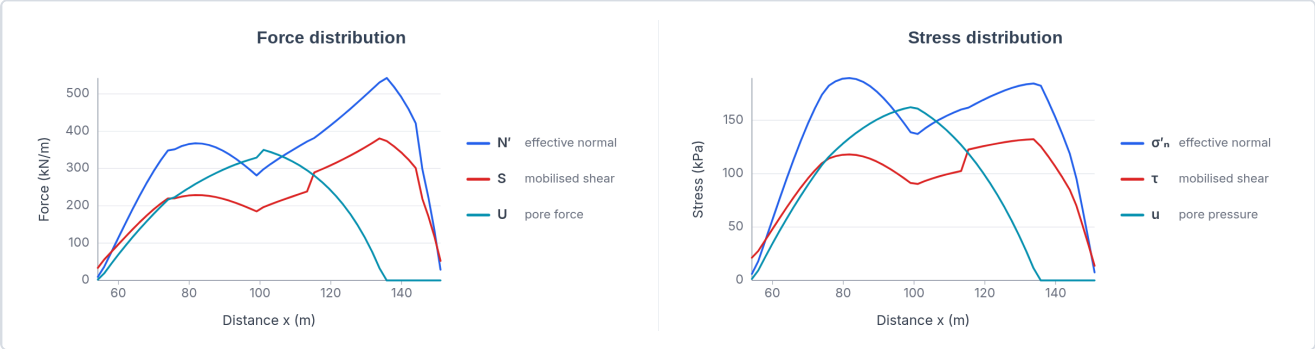


Figure 2. Distribution of the solved per-slice results along the critical surface (Slide2 #20). Left: the slice forces, effective normal N', mobilised shear S and pore force U (kN/m). Right: the corresponding base stresses, effective normal σ'_n, shear τ and pore pressure u (kPa), the same quantities per unit base length. Both are read directly from the slices of Figure 1, exposing the full internal solution rather than only the factor of safety.

2. Verification methodology

2.1 Sources

1. **GeoStudio SLOPE/W 2D Verification Manual**: the ACADS study problems (Giam & Donald, 1989) and classic literature slopes. Eight limit-equilibrium cases were replicable from tabulated inputs: five circular, plus three non-circular variants of the ACADS weak-layer problem (block search, specified surface, and a block search carrying a piezometric surface and a linearly-varying surcharge).
2. **Rocscience Slide2 Slope Stability Verification Manual** (2022): 111 verification problems drawn from the ACADS study and the wider literature (Arai & Tagyo 1985; Yamagami & Ueta 1988; Greco 1996; Chen & Shao 1988; Low 1989; Fredlund & Krahn 1977; Baker 2003; Duncan & Wright 2005; Prandtl 1921; and others).

2.2 Protocol

- Each problem was rebuilt **exclusively from tabulated coordinates and properties** (or coordinates computable exactly from the stated slope height and angle). Problems whose geometry, water table or pore-pressure field exists only as an un-dimensioned figure were rejected rather than digitized by eye. Model bases are treated as impenetrable by a bedrock keep-out that follows the soil mass's lower envelope.
- Problems were solved with all seven methods. Where the manual analyzed a *single specified circle*, that exact circle was analyzed; otherwise the engine's automatic search located the critical circle (40 × 40 centers × 25 radii plus refinement; 30–40 slices). Where a manual's search was deliberately restricted (Slide2 #20 uses a "focus object" at the toe), the restriction was reproduced with the engine's entry–exit range limits. Where the published failure surface is **non-circular**, the tabulated surface is analyzed directly as a polyline (Slide2 #8 / SLOPE/W §2.8); where the manual block-searches a weak seam, the engine's two-window block search reproduces it (Slide2 #7 / SLOPE/W §2.7, and, with a piezometric surface and a linearly-varying surcharge layered on top of a dipping seam, Slide2 #9 / SLOPE/W §2.9); and Slide2 #22's **composite circular** surface, its specified circle running along a thin weak layer, is reconstructed exactly (the tabulated circle's two arcs joined by the weak-seam flat) and an-

d (they presume the common-center moment arm) and the GLE-family/Janbu values are compared instead. Tension cracks were modeled as crack-bottom polylines (taken verbatim from the manual's stated line, or derived from its stated depth), truncating every trial surface with a vertical face and applying the hydrostatic thrust where the crack is stated water-filled. Reinforcement elements enter through the engine's force-resolution: each element's available force $F = \min(\text{failure modes})$ over tendon/tensile capacity, grout or interface pullout, facing/plate strip-through, and (for piles) lateral shear, is resolved at the slip-surface crossing into a base-tangential part $T_{\parallel}$ (adds to the resisting shear) and a base-normal part $T_{\perp}$ (raises the base normal force, and hence friction), with passive elements adding to the resisting side and active pre-tensioned elements subtracting from the driving side (Slide2 parity).

- **Primary comparison:** our Bishop ↔ published Bishop; where no Bishop value is published, our Morgenstern–Price ↔ published GLE/Spencer. Literature "reference" values of a different mechanism (e.g. planar solutions) are reported but never counted as deviations. Our Janbu (which always applies f_0) is compared against published *Janbu corrected* columns.
- Every replicated case is exported as a machine-readable model input file, available for download, and the whole campaign is scripted end-to-end, so the study is reproducible.

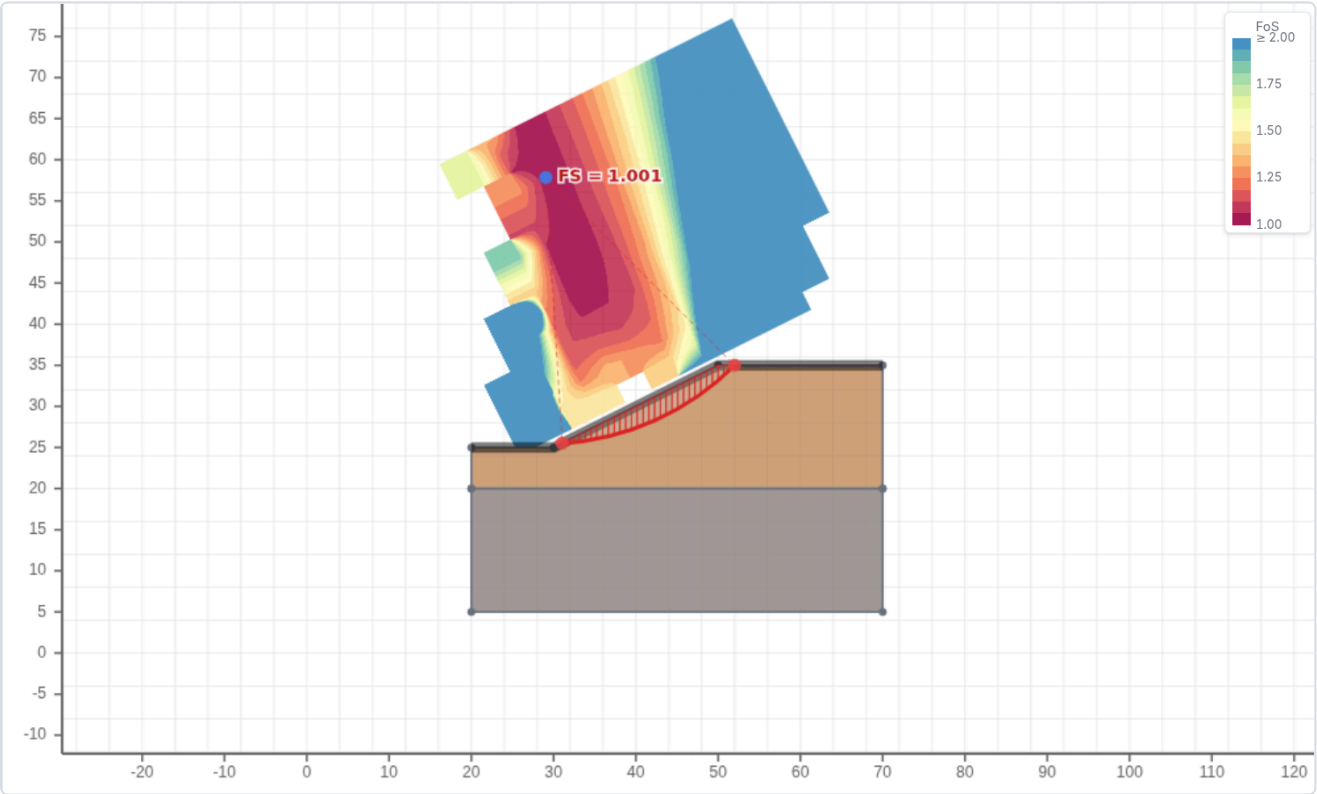


Figure 3. Search coverage on the ACADS 1(a) slope, rendered as a minimum factor-of-safety heat map: each point is tinted by the lowest factor of safety of any admissible trial circle passing through it (deep red at the critical zone, FoS ≈ 1.0, grading through the spectral scale to blue for the safer surrounding ground), beside its color-bar legend, with the critical surface and its slices highlighted. The application's fine grid preset supplies the field shown; the scripted campaign uses a denser sweep (40 × 40 centers × 25 radii plus local refinement) of the same search space.

2.3 Independence checks

Two safeguards were used against self-confirmation. First, extraction and solving are decoupled: case specifications are plain data, validated by schema and geometry checks before solving. Second, for the one case whose published values could not be matched (§4.3), the engine was cross-

checked by an **independent slice-by-slice Bishop hand calculation** implemented separately from the engine, plus a Culmann planar bound.

3. Results

3.1 SLOPE/W (ACADS) suite

Case	Method	Reference	Published (SLOPE/W)	Ours	Δ
ACADS 1(a) simple slope	Bishop	1.000	0.993	0.987	−0.6 %
	Morgenstern–Price		0.993	0.986	−0.7 %
	Janbu†		0.939	0.989	+5.3 %†
	Ordinary‡		—	0.943	—
ACADS 1(b) tension crack§	Bishop	1.65–1.70	1.664	1.594	−4.2 %§
	Morgenstern–Price		1.660	1.590	−4.2 %§
	Janbu†		1.471	1.492	+1.4 %
	Ordinary‡		—	1.521	—
Arai & Tagyo homogeneous	Bishop	1.451	1.417	1.404	−0.9 %
	Morgenstern–Price		1.414	1.409	−0.4 %
	Janbu†		1.322	1.417	+7.2 %†
	Ordinary‡		—	1.343	—
ACADS 1(c) three-layer	Bishop	1.390	1.413	1.393	−1.4 %
	Morgenstern–Price		1.382	1.367	−1.1 %
	Janbu†		1.260	1.347	+6.9 %†
	Ordinary‡		—	1.217	—
ACADS 1(d) three-layer + $k_h = 0.15$	Bishop	1.000	1.016	1.005	−1.1 %
	Morgenstern–Price		0.989	0.982	−0.7 %
	Janbu†		0.897	0.962	+7.2 %†
	Ordinary‡		—	0.935	—
ACADS 3(a) weak layer, block search¶	Morgenstern–Price	1.24–1.27	1.261	1.200	−4.8 %¶
	Janbu†		1.229	1.234	+0.4 %
	Bishop‖		1.269	—	—

Case	Method	Reference	Published (SLOPE/W)	Ours	Δ
ACADS 3(b) weak layer, specified surface	Morgenstern–Price	1.34	1.261	1.253	−0.6 %
	Janbu†		1.197	1.283	+7.2 %†
	Bishop‖		1.259	—	—
ACADS 4 weak layer, external loading**	Morgenstern–Price	0.688	0.689	0.735	+6.7 %**
	Janbu†**		0.671	0.848	+26.4 %**
	Bishop‖		0.692	—	—

Reference = the accepted ACADS / original-author answer, where the manual states one.

† Our Janbu always applies the f_0 depth correction, whereas SLOPE/W's published "Janbu" column is the uncorrected force-equilibrium value; the systematic +5–7 % reflects that correction ($f_0 \approx 1.05$–1.07 here), not an engine deviation. In the Slide2 suite (§3.2), where a published "Janbu corrected" column exists, the same implementation agrees to a mean of 2.3 % across the Janbu-corrected comparison set (14 cases; 13 within 5 %, the exception being case #9's non-circular block search, §3.2).

‡ The SLOPE/W manual publishes no Ordinary (Fellenius) values for these cases; ours are reported for completeness and are, as expected, the most conservative of the methods.

§ ACADS 1(b), the 1(a) slope with $c' = 32$ kPa, $\varphi' = 10°$ and a water-filled tension crack, is the one case where the two commercial manuals themselves disagree: SLOPE/W publishes Bishop 1.664 (crack depth "about 3.6 m") while Slide2 publishes Bishop 1.596 for the identical problem (crack line 4.0 m below ground), a 4.1 % spread between the two programs. Our engine, run with each manual's own crack definition, gives 1.588 against Slide2's 1.596 (−0.5 %, see §3.2 case #2) and 1.594 against SLOPE/W's 1.664 (−4.2 %); the ACADS reference answer is the range 1.65–1.70. The crack-depth difference itself moves our F by only ~0.3 %, so the spread reflects the two programs' different crack treatments rather than the inputs.

*¶ ACADS 3(a)/(b), the two-material slope with a thin weak seam, are the manual's non-circular weak-layer pair: 3(b) analyzes a tabulated 4-vertex surface transecting the seam (analyzed directly as a polyline, −0.6 %), while 3(a) block-searches the seam. On 3(a) our two-window block search converges to a **different critical block** than GeoStudio's, one hugging the seam's base over a longer run, with a **lower** (more critical, conservative-side) factor of safety: M-P 1.200 vs the published 1.261 (−4.8 %). The specified-surface companion pins the solver itself to −0.6 %, isolating the difference to the search landscape, and the Slide2 variant of the identical problem behaves the same way (§3.2, case #7).*

‖ Bishop and Ordinary presume a circular moment arm and are gated off non-circular surfaces: the engine reports no value rather than a silently-wrong one; the manuals' generalized-Bishop values are shown for reference.

*** ACADS 4 (issue #20), the fourth member of the weak-layer family, and the campaign's first case exercising a **linearly-varying (trapezoidal) surcharge**: the same two materials as 3(a)/(b), but the weak seam now **dips** across the full model width (not the horizontal band of 3(a)/(b)), carries a piezometric surface (Table 21), and the ground supports two surface loads (Table 20): a uniform 20 kN/m² bench load and a trapezoidal load rising 20⟶40 kN/m² across the plateau. Our block search (the same non-circular technique as 3(a)) finds a critical surface at M-P 0.735, **+6.7 %** above GeoStudio's published M-P (0.689) and its published Bishop (0.692, reference 0.688), the campaign's other primary comparison beyond 5 %, alongside 3(a). Unlike 3(a), where both programs searched non-circular surfaces and ours found the more critical one, here the divergence runs the other way: GeoStudio's manual states its search was restricted*

*to **circular** surfaces (consistent with a published Bishop value existing at all, since Bishop is gated off non-circular surfaces everywhere else in this pair), while the dipping seam's true critical mechanism is non-circular. Reproducing that non-circular mechanism is exactly what the identical problem's Slide2 publication independently confirms: its own block-searched GLE value is 0.720, and our M-P matches it to **+2.1 %** (§3.2, case #9), closer than either program's circular answer. This is a block-vs-circular search-landscape difference, not a solver defect. Our Janbu, which always applies the f_0 correction (†) and inherits the same non-circular divergence, is +26.4 % above GeoStudio's Janbu (0.671), reported for transparency, not as a headline comparison.*

The engine reproduces not only the values but the published *ordering* between methods (M-P marginally below Bishop on the layered and seismic cases).

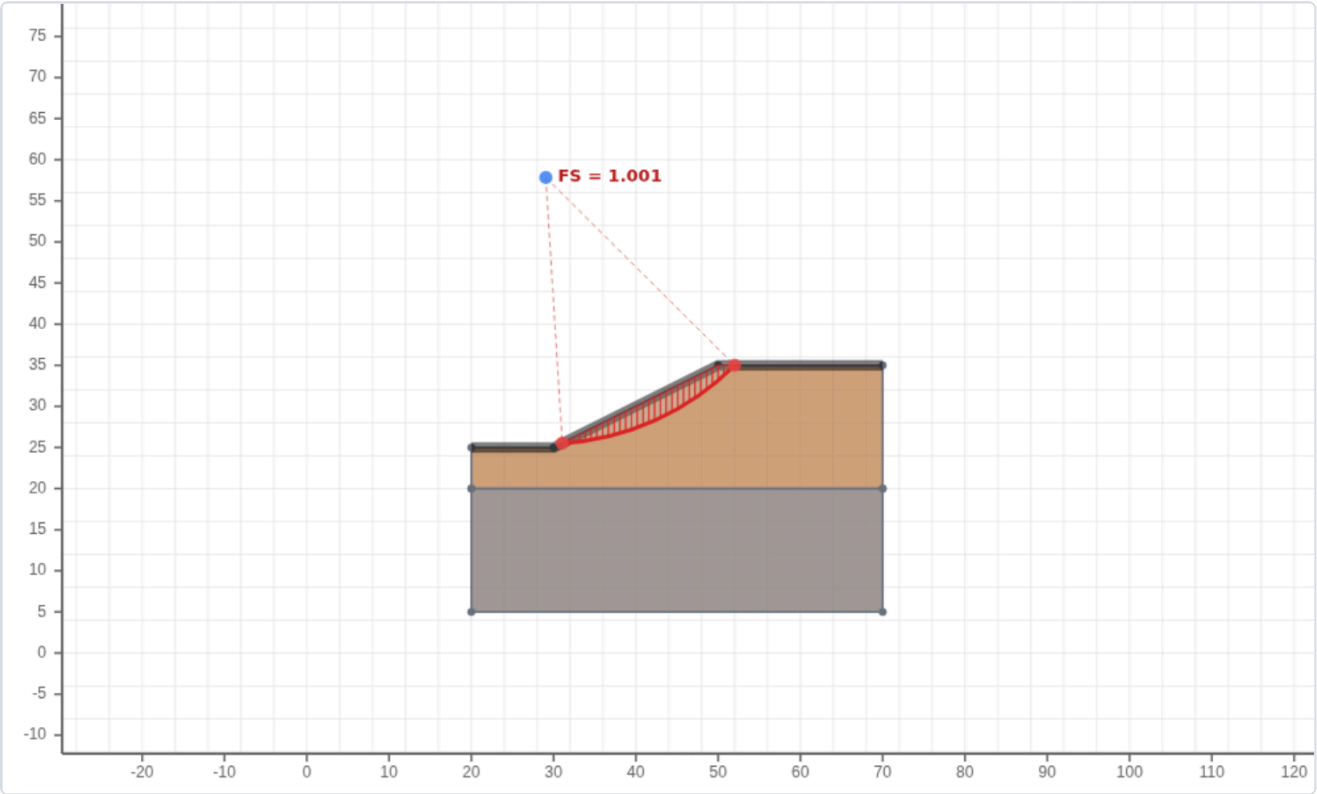


Figure 4. ACADS 1(a) simple slope solved in the application: critical circle, slice discretization and center/radius construction. The interactive fine-grid preset shown reports F = 0.998; the campaign's denser scripted sweep refines the same minimum to 0.987 (published: 0.993).

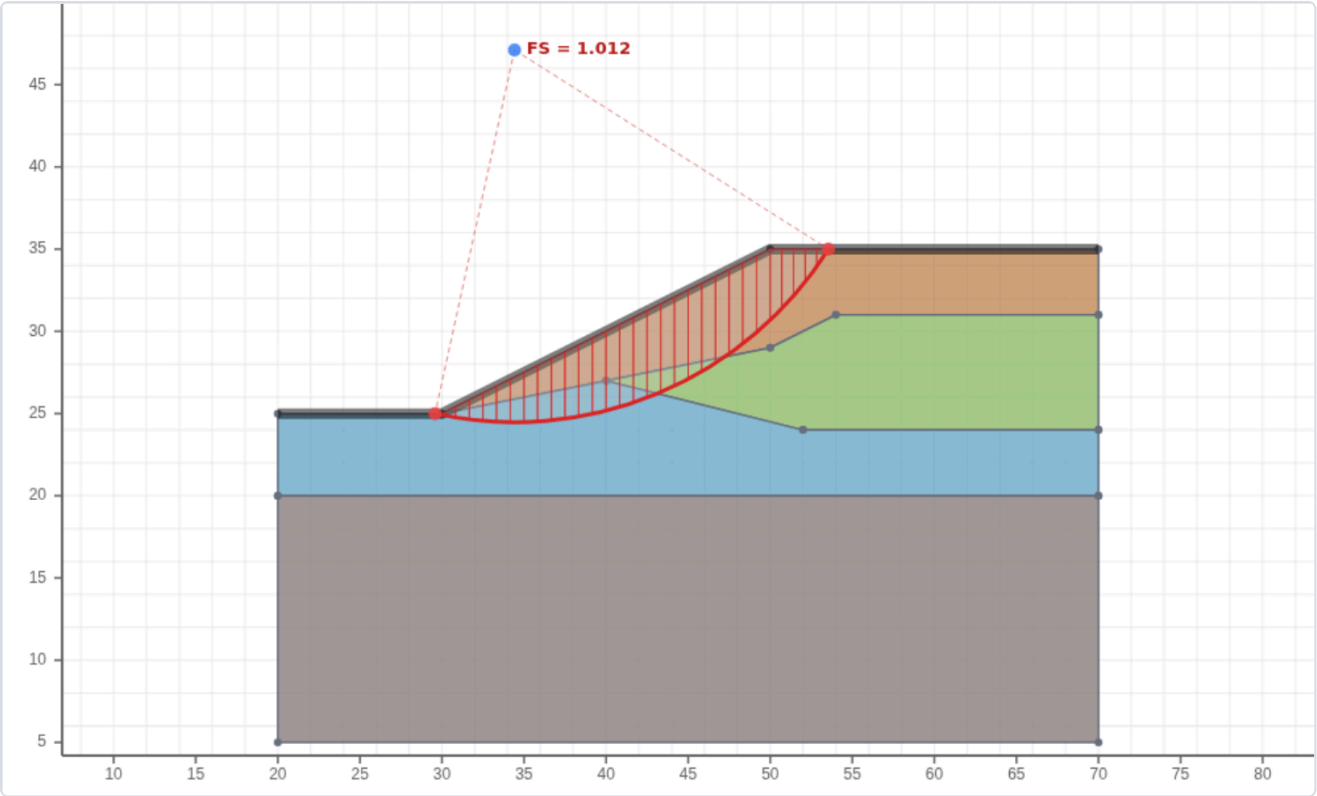


Figure 5. ACADS 1(d): three soil layers with pseudo-static loading k_h = 0.15. The critical circle cuts all three strata; F = 1.005 (published: 1.016, −1.1 %). The seismic direction is chosen automatically by solving both shaking directions.

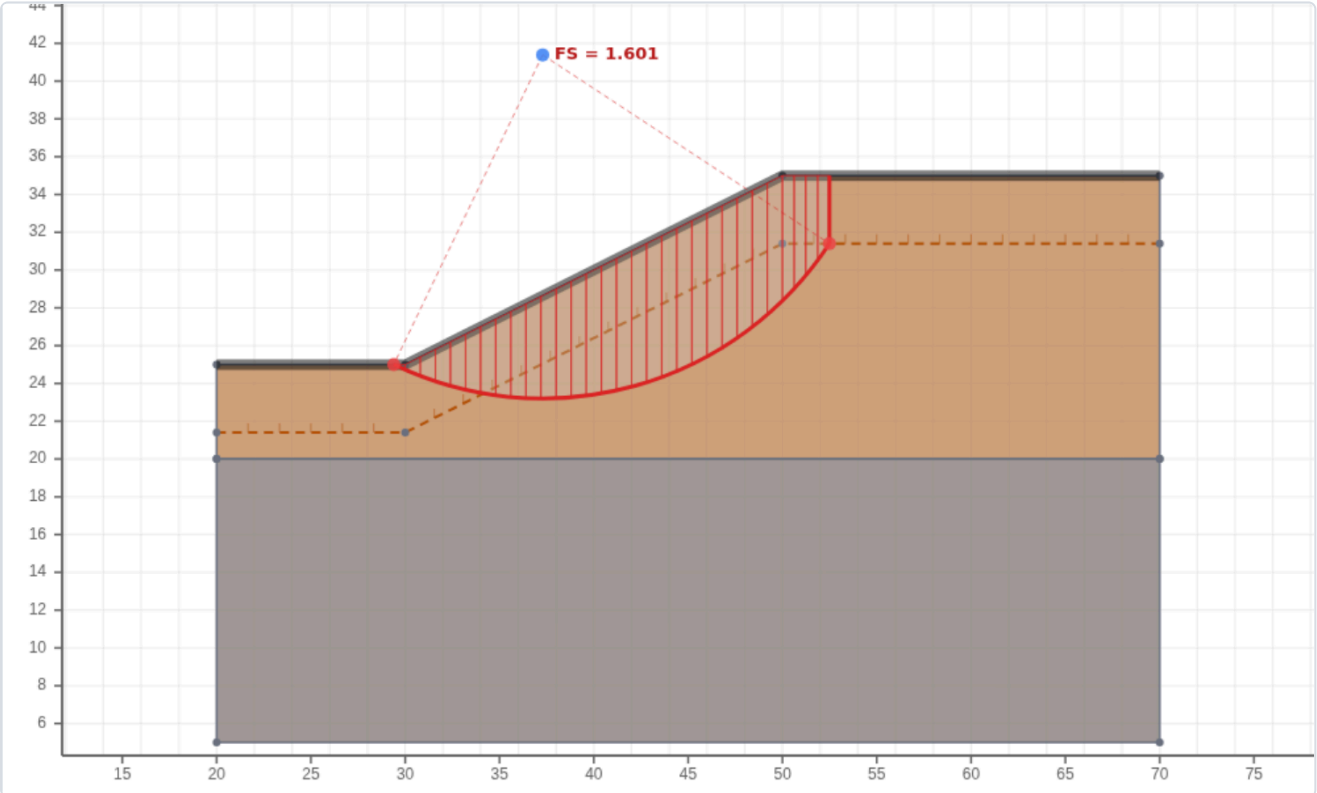


Figure 6. ACADS 1(b) solved in the application: the dashed line 3.6 m below the ground marks the crack bottom (ticks pointing into the cracked zone). The critical circle is truncated where it crosses the line (the red vertical segment is the crack face, carrying the hydrostatic thrust of the water filling the crack) and the slices stop at the face. The interactive fine-grid search reports F = 1.607; the campaign's denser sweep refines it to 1.594.

3.2 Slide2 suite

Of the 111 problems, **38 problems are replicated** (several with multiple sub-case variants → 56 extracted sub-cases, of which 3 were excluded during validation with documented evidence; see §4). The final population: **53 solved cases, 51 with a primary published comparison, zero failures**, the cases beyond the circular set being #54's reinforced (with-pile) variant (§3.3), the non-circular weak-layer trio #7/#8/#9, the composite-surface pair #22 (dry and r_u), and the depth-varying-strength case #23. Four reinforcement capability-demonstration cases are reported separately in §3.3 and are not counted in these verification statistics.

Comparison	n	mean |Δ|	median |Δ|	max |Δ|	≤ 2 %	≤ 5 %
Bishop ↔ Bishop	41	**1.0 %**	0.7 %	4.7 %	37/41	41/41
M-P ↔ GLE/Spencer	43	1.5 %	0.8 %	6.8 %	33/43	39/43
Spencer ↔ published Spencer	43	1.9 %	0.9 %	8.5 %	31/43	37/43
Janbu (f_0) ↔ Janbu corrected	14	2.3 %	0.8 %	15.5 %	10/14	13/14
Ordinary ↔ Ordinary	8	0.2 %	0.2 %	0.7 %	8/8	8/8

Corps of Engineers and Lowe–Karafiath have no published columns in the replicated set (only the excluded rapid-drawdown problems #95–#99 carry them); they are consistency-verified, not benchmark-verified. The Ordinary row excludes #23, whose published Ordinary value belongs to that method's own tabulated critical circle rather than the circle the case analyzes; the like-for-like comparison on the manual's own Ordinary circle is −0.2 % (see the #23 result below). The Janbu row's new maximum (15.5 %) is case #9's non-circular block search, layering the same f_0-correction offset (†, §3.1) on top of a block-vs-circular search-landscape divergence; every circular case in the row remains within 4.2 % (see §4.2).

The replicated set spans: homogeneous and multi-layer slopes (up to 6 strata); weak seams; dry, phreatic and r_u pore-pressure regimes; **tension cracks, dry and water-filled**; pseudo-static seismic loading up to k_h = 0.4 (alone and combined with r_u = 0.5); metric and imperial unit systems; undrained (φ = 0) profiles, including **depth-varying undrained strength**; embankments on soft foundations; dam sections (Talbingo, James Bay); searched and manual-specified slip circles; **non-circular surfaces** (a predefined weak-seam polyline, two block searches, and a composite circular surface running along a weak layer); and a **linearly-varying (trapezoidal) surcharge**. The complete per-case model configurations and factor-of-safety comparison are given in **Appendix A**, and each case's machine-readable model input file is available for download.

Notable individual results:

- **Slide2 #3 / #4 (ACADS 1(c) / 1(d): the three-layer slope, static and seismic)**: one non-homogeneous three-layer profile (Soil 1 c' = 0, φ' = 38°; Soil 2 c' = 5.3 kPa, φ' = 23°; Soil 3 c' = 7.2 kPa, φ' = 20°; all γ = 19.5 kN/m^3) solved dry (#3) and under pseudo-static loading k_h = 0.15 (#4). Dry: **Bishop 1.392 vs Slide 1.405 (−0.9 %)**, Spencer 1.363 vs 1.375, M-P 1.364 vs GLE 1.374. Seismic: **Bishop 1.007 vs 1.016 (−0.9 %)**, the critical circle cutting all three strata. #3 is the Slide2 twin of the SLOPE/W ACADS 1(c) problem (§3.1, Bishop −1.4 %); its accepted reference is Giam's **1.39**; the manual's Table 3.2 note misprints this as 1.65, a transcription of Problem #2's water-filled-crack reference, corroborated by the manual's own mean Bishop of 1.406. The three-layer interior interface vertices, unlabeled in Figure 3.1, are read off its calibrated axes as (40, 27), (50, 29), (54, 31), (52, 24).

- **Slide2 #20** (Greco 1996 ex. 5: four materials, thin weak seam, water table): the published circular value (Bishop 1.087) derives from a search *focused at the toe*. Reproducing that restriction through the engine's entry–exit limits gives **1.085 (−0.1 %)**.

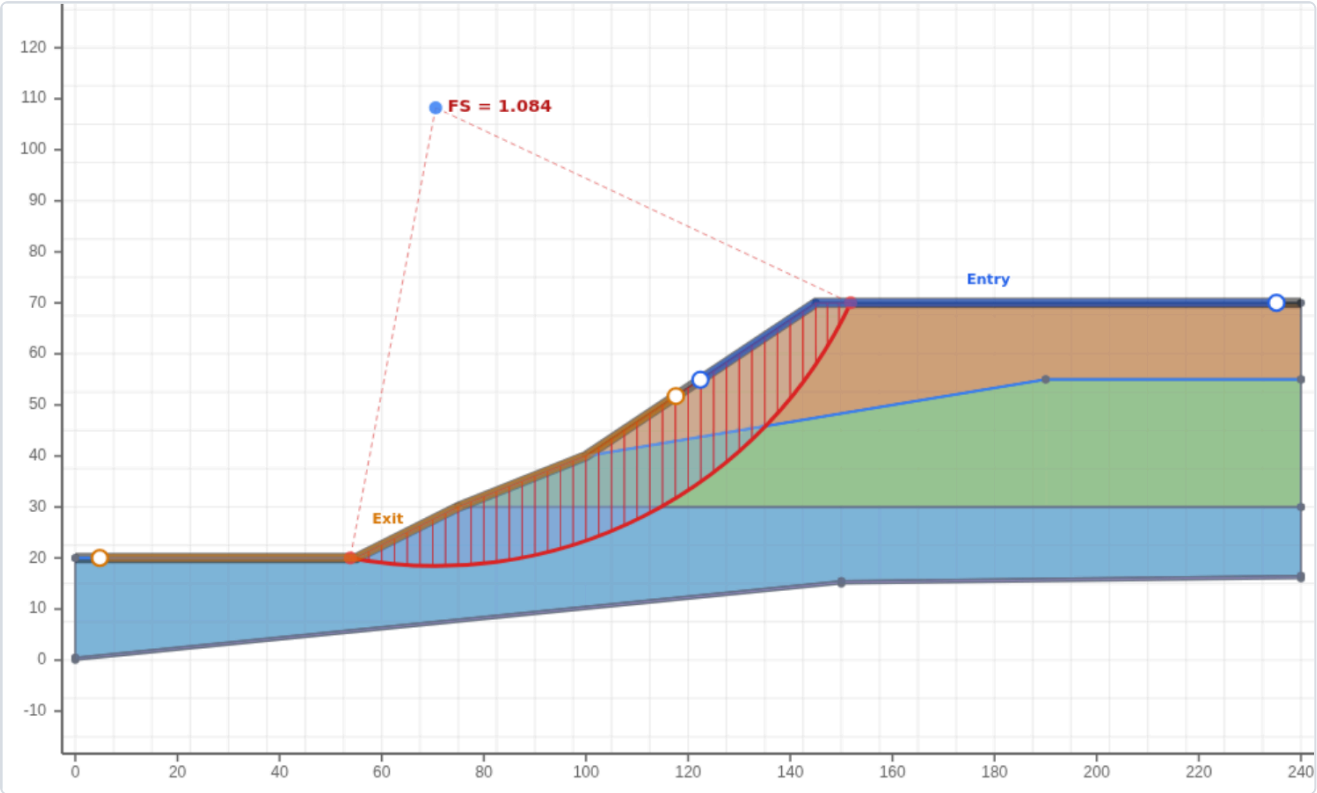


Figure 7. Slide2 #20 reproduced interactively: four strata with a thin weak seam above bedrock and a water table at ground level on the lower reach. The manual's toe-focused search is expressed as entry–exit daylight windows (entry 100–200 m on the crest, exit 54–56 m at the toe, marked on the ground surface); the search returns F = 1.087 against the published 1.087.

- **Slide2 #2** (ACADS 1(b): water-filled tension crack, depth stated as $2c/(\gamma\sqrt{K_a})$): searched critical circle with the crack truncation and its hydrostatic thrust gives Bishop **1.588 vs published 1.596 (−0.5 %)**, M-P 1.584 vs 1.592, Janbu(f_0) 1.477 vs Janbu-corrected 1.489.
- **Slide2 #52** (Zhu & Lee 2002: four materials, dry tension crack at the crest, specified circles, dry and wet): all four circular sub-cases within 1.9 % on Bishop; the wet Surface-3 case only reconciled after reading the first water-table row of Table 52.2 as (−20, 0), the physically sensible left-edge point, rather than the printed (0, −20); with that correction an independent hand calculation reproduces the published 1.176 to +0.3 %.
- **Talbingo Dam** (4 zones): searched case +0.9 %; the manual's specified circle **+0.1 %**.
- **Fredlund & Krahn / Low / Prandtl-family cohesive cases** (#78a–f): six sub-cases all within 1.3 %.
- **Spencer's five critical-circle >5 % outliers** (078a, 078c, 078e, 014, 015: 6.2–8.0 % on the toe-circle members of the #78 series, 5.1–6.7 % on #14/#15; all auto-**search** cases) are a critical-circle search-landscape effect, not a Spencer-solver defect. Evidence: the #78 series' **specified**-circle siblings (078b, 078d, 078f, the same geometry and soils on the manual's own circle) agree with the published Spencer column to −0.6 %, −0.7 % and −0.9 % respectively, and on every one of the five outlier cases our Spencer tracks our own M-P on the *same* auto-search circle to within 1.6 % (mean ≈0.5 %, two of the five under 0.01 %). The manuals' own tabulated values for #14/#15 already disagree internally between their circular-search Spencer and GLE columns by 5–7 %, consistent with a flat, multimodal $F(\text{circle})$ surface on these $\varphi = 0$

/layered geometries where independent optimizers converge to different local minima rather than a systematic solver error.

- Combined seismic + pore pressure (#62b, k_h = 0.4, r_u = 0.5): **0.0 %**.
- **Slide2 #8 / #7 (ACADS 3, weak-layer non-circular pair)**: #8's tabulated 4-vertex surface, transecting a 0.5 m weak seam, is analyzed directly as a polyline: **M-P 1.254 vs published GLE 1.262 (−0.6 %)**, Spencer 1.266 vs 1.277 (−0.8 %), Janbu(f_0) 1.283 vs Janbu-corrected 1.294 (−0.9 %). The companion *searched* problem #7 reproduces the manual's block search with the engine's two-window search: it converges to a **different critical block**, hugging the seam over a longer run, with a *lower* factor of safety than the manual's own (Spencer 1.214 vs 1.246, −2.6 %; M-P 1.200 vs GLE 1.275, −5.9 %, one of the campaign's two primary comparisons beyond 5 %). Finding a more critical admissible surface is the conservative direction for a search; the GeoStudio variant of the identical problem diverges the same way (−4.8 %, §3.1), and the specified-surface companions pin the solver itself to −0.6 %.
- **Slide2 #9 (ACADS 4: weak layer, water table and a trapezoidal surcharge)**: the fourth member of the ACADS weak-layer family, and the campaign's first case with a **linearly-varying (trapezoidal) surcharge** (issue #20): the same two materials as #7/#8, but the weak seam **dips** across the full model width, carries a piezometric surface, and the ground supports a uniform 20 kN/m² bench load plus a trapezoidal load rising 20→40 kN/m² across the plateau. The engine's block search, the same non-circular technique as #7, finds a critical surface at **M-P 0.735 vs published GLE 0.720 (+2.1 %)**, Spencer 0.695 vs 0.760 (−8.5 %), Janbu(f_0) 0.848 vs Janbu-corrected 0.734 (+15.5 %); the accepted reference is 0.78 (Giam), and the manual separately tabulates a Slope-2000 reference GLE of 0.6878. This is the closest of the two suites' answers to our own: the companion GeoStudio §2.9 problem (§3.1), which restricted its search to circular surfaces, reads 6.7 % higher, a block-vs-circular search-landscape difference, not a solver defect, and the campaign's other primary comparison beyond 5 %.
- **Slide2 #22 (Fredlund & Krahn 1977 weak-layer slope: composite surface, dry and r_u)**: the canonical weak-layer benchmark's **composite circular** surface, the specified circle (x_c = 120, y_c = 90, R = 80) dropping to a thin weak seam and running along it, is reconstructed exactly as Slide computes it (the two circular arcs joined by the weak-seam flat) and analyzed as a predefined polyline. Dry: **M-P 1.392 vs published GLE 1.372 (+1.4 %)**, Spencer 1.400 vs 1.382 (+1.3 %). With r_u = 0.25 on both soils: **M-P 1.139 vs 1.114 (+2.3 %)**, Spencer 1.149 vs 1.124 (+2.2 %), exercising r_u pore pressure on a non-circular surface. Fredlund & Krahn's own values (Spencer 1.373 dry, 1.118 wet) bracket the same numbers.
- **Slide2 #23 (Low 1989: depth-varying undrained strength)**: the lower soil's undrained strength rises linearly from 15 kN/m² at its top to 30 kN/m² at its base, the engine's depth-varying c_u model. On the manual's own tabulated Bishop critical circle: **Bishop 1.136 vs Slide's 1.192 (−4.7 %, the campaign's largest Bishop deviation)**, but the published sources themselves span the second decimal on this benchmark: Low's original Bishop is 1.14 (**we match to 0.4 %**) and Kim (2002) reports 1.17. On the manual's tabulated *Ordinary* critical circle, our Ordinary converges to 1.367 vs the published 1.370 (−0.2 %). The constant-inclination force methods (Spencer, Corps, Lowe–Karafiath) do not converge on this deep $\varphi = 0$ surface and are unpublished for the problem.

3.3 Reinforcement

The engine models four reinforcement element types (grouted **anchors**/tiebacks, fully-bonded **soil nails**, horizontal **geosynthetic** sheets, and laterally-loaded **piles**), each resolved at the slip-surface crossing as described in §2.2. Published *circular* reinforced benchmarks are scarce: the soil-nailed and tied-back walls of the Slide2 suite (#47, #48, #49, #58–60) are analysed on **planar** failure surfaces the circular engine does not represent, and the geosynthetic-reinforced embankments (#30–32, #39) carry figure-only tension cracks and depth-varying undrained strength. One published reinforced problem is fully circular and tabulated, and it is reproduced here; the four element types are then demonstrated on a common slope.

Slide2 #54: stabilising micro-piles (Yamagami 2000). The homogeneous slope of case #54 (c' = 4.9 kPa, φ' = 10°, γ = 15.68 kN/m^3) is reinforced by a single row of micro-piles at 1 m horizontal spacing, each carrying a lateral shear strength of 10.7 kN. Modelled as a passive shear dowel resolving tangent to the slip surface, placed at the slope head (x = 7.5 m, read from the manual's Figure 54.3) and extending below the critical arc, the pile develops its full 10.7 kN/m shear on the critical surface and lifts the factor of safety from the unreinforced **1.102** (case #54, §Appendix A) to **Bishop 1.209 vs the published Slide 1.193 (+1.4 %)** (Yamagami 1.20). The result is robust across the slope-head region (piles at x = 6–7.5 m all give 1.209–1.210); analysing the manual's own reported with-pile circle directly gives 1.211 (+1.5 %). A single pile row only stabilises the surfaces that cross it: placed past the crest break, a shallower surface daylighting in front of the pile bypasses it and governs, which is itself a faithful reproduction of the mechanism.

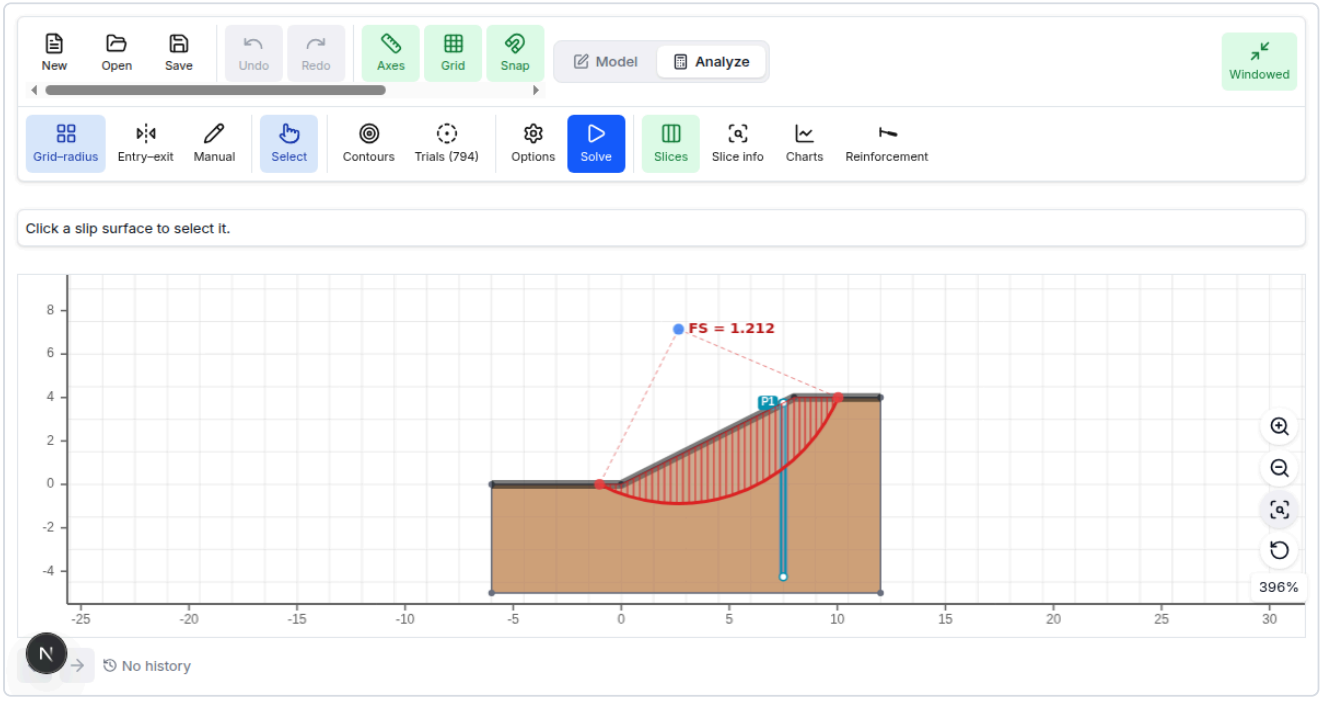


Figure 8. Slide2 #54 reinforced with a single micro-pile row (P1, the vertical blue element at the slope head), solved in the application. The critical circle is truncated to the deep mechanism the pile stabilises; the pile shaft crosses the slip surface and develops its 10.7 kN/m lateral shear, raising the factor of safety to F = 1.212 on the interactive fine grid (the campaign's denser sweep refines it to 1.209; published Slide 1.193).

Capability demonstration (four element types). To exercise the full force-resolution, each element type is applied, one at a time, to the #54 slope on its unreinforced critical circle (Bishop ≈ 1.100), so the four are compared on identical geometry. This is an illustration of the engine's beh-

aviour, not a published-benchmark comparison; there is no published deviation to report.

Element	Governing mode	F (kN/m)	$T_{\parallel}$ (kN/m)	$T_{\perp}$ (kN/m)	FoS (unreinf. 1.100)
Grouted anchor	strip-through	40.0	+27.9	+28.7	1.642
Soil nail	tensile	40.0	+26.7	+29.8	1.442
Geosynthetic sheet	tensile	30.0	+29.1	+7.3	1.427
Pile (shear dowel)	shear	10.7	+10.7	+0.0	1.217

Each element's available force is limited by a different governing mode; $T_{\parallel}$ adds directly to the resisting shear and $T_{\perp}$ raises the base normal force (and hence friction). The pile carries only a tangential shear ($T_{\perp} = 0$); the anchor and nail, inclined into the mass, develop a large normal component; the geosynthetic sheet is nearly tangential.

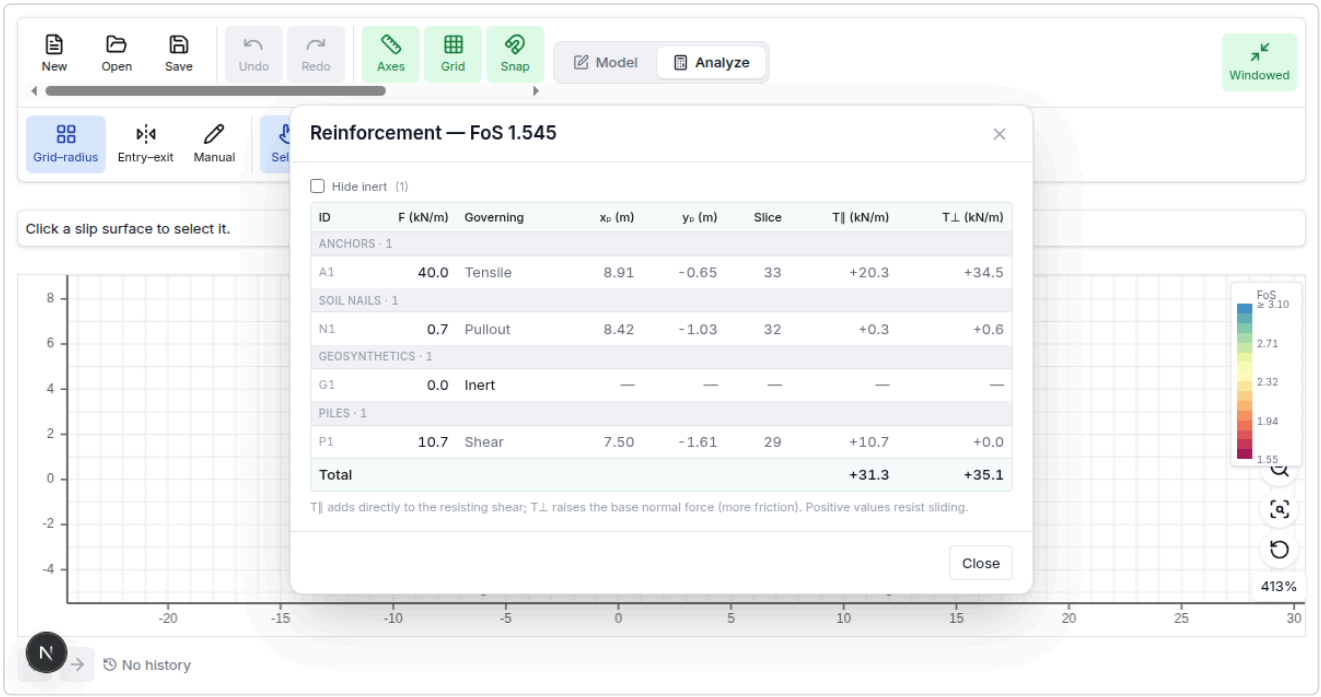


Figure 9. The application's per-element reinforcement results on a slope carrying all four element types (anchor A1, nail N1, geosynthetic G1, pile P1). Each element reports its available force F, governing failure mode, slip-surface crossing point (x_p, y_p) and slice, and the base-tangential/normal components $T_{\parallel}/T_{\perp}$ entering the factor-of-safety ratio, with a running total; an inert element (one not crossing the critical surface) is flagged and can be filtered out.

4. Discussion

4.1 Method-specific observations

The Bishop agreement (mean 0.9 %) is within the spread typically observed *between* commercial implementations of the same method, and small residuals are dominated by search discretization rather than the force system: specified-circle cases agree more tightly (e.g. #6 at 0.1 %, #78b/d/f ≤ 1 %) than searched ones. The M-P comparison carries the additional variance of comparing one GLE variant against another (Slide2's GLE and Spencer differ from each other by similar margins in the manual itself).

The Ordinary/Fellenius comparison exposed a convention split worth recording: with the classical pore term $N' = W\cos\alpha - u\ell$ (ℓ = base length), the two deep wet cases (#21b, #52d) deviated by 5–16 % while every dry case matched, the classical form's known over-conservatism under high pore pressure on steep bases. Switching to the **corrected Fellenius form** $N' = (W - ub)\cos\alpha$ (Duncan & Wright 2005, the convention the commercial manuals publish) brought all eight Ordinary comparisons to within 0.7 % without changing any dry result.

4.2 Janbu correction

The engine always applies the f_0 correction; the published *Janbu simplified* columns are therefore systematically below our Janbu values, and only the *Janbu corrected* columns are compared: 13 of 14 within 5 % (max 4.2 % on the circular set). The exception is #9's non-circular block search, whose dipping-seam mechanism compounds the usual correction offset with a block-vs-circular search-landscape divergence to +15.5 % (§3.2, §3.1 §2.9).

4.3 A discrepant published case

For Slide2 **#44a** (Baker 2003 ex. 1, linear Mohr-Coulomb fit), the published values (Janbu 1.469 / Spencer 1.536) could not be reproduced from the manual's own figure geometry ((0,0)–(6.43,6)–(20,6)) and tabulated properties (c' = 5.3 kPa, φ' = 23°, γ = 19.5 kN/m^3). An independent slice-by-slice Bishop hand calculation **on the manual's own reported critical circle** gives F = 1.041, identical to the engine, and the Culmann planar bound is 1.283, an upper mechanism that already excludes 1.469 for a well-searched circle family. The companion rows of the same problem (power-curve and iterated-M-C materials) *are* consistent with the stated 43° geometry, indicating the published M-C row reflects Baker's original geometry rather than the manual's figure. The case is reported without a deviation statistic.

4.4 Scope exclusions

73 of the 111 Slide2 problems remain unreplicated: most are outside the engine's current scope, the rest blocked by inputs that exist only as figures. The dominant categories: non-circular problems requiring general random-path / multi-modal surface optimizers (the engine's non-circular support is a predefined polyline plus a targeted weak-layer block search); pore-pressure grids and FE-seepage fields; power-curve ($\tau = A\,\sigma'^{b}$) strength envelopes and user-defined interslice force functions; ponded/submerged conditions; staged rapid drawdown; support-element walls on planar surfaces; probabilistic problems whose geometry is never tabulated; the engine itself now carries a seeded MC/LHS probabilistic layer (§1), but none of the manual's four probabilistic problems (#29, #33–#35) is faithfully extractable; and problems whose inputs are only drawn, not tabulated. Several categories have moved from fully excluded to *partially replicated* as the engine gained the corresponding feature during this campaign: **tension cracks** (#2 and the circular sub-cases of #52), **reinforcement** (#54's micro-pile variant, §3.3), **non-circular surfaces** (#7's block search, #8's predefined polyline, #9's dipping-seam block search, and #22's composite weak-layer surface), **depth-varying undrained strength** (#23), and **external loading** (#9's linearly-varying trapezoidal surcharge, issue #20, layered on top of its non-circular mechanism). In each instance the problems still excluded from that category remain so for separate, re-verified reasons (planar-surface support walls, figure-only geometry, non-tabulated strengths). Three extracted sub-cases were excluded during validation: two razor-thin "infinite-slope mechanism" circles whose arcs sit below the geometric resolution of figure-annotated coordinates, and one case whose piezometric line (approximating an FE seepage solution) is drawn but never tabulated.

5. Limitations

- The engine's non-circular capability is a **predefined polyline** surface plus a targeted **weak-layer block search**; general random-path / surface-altering optimizers, and the benchmark problems that require them, are not addressed. Block-search comparisons carry a search-landscape caveat: two independent implementations can converge to different critical blocks on the same seam. On ACADS 3(a)/#7 our search lands on the more critical (conservative) side of both manuals' answers (§3.1 ¶, §3.2 case #7); on ACADS 4/§2.9/#9 it lands on the *less* critical side of GeoStudio's circular-search answer but within 2.1 % of Slide2's own independently-published block search on the identical problem (§3.1 §2.9, §3.2 case #9), a reminder that "conservative" is a property of the specific search comparison, not a guaranteed direction.
- On deep $\varphi = 0$ undrained surfaces the constant-interslice-inclination force methods (Spencer, Corps of Engineers, Lowe–Karafiath) may fail to converge (#23); the moment methods are unaffected.
- Pore-pressure grids, B-bar and staged rapid drawdown, ponded water above the ground surface, power-curve ($\tau = A\,\sigma'^{b}$) envelopes and user-defined interslice force functions are not modeled.
- The searched-case comparisons inherit each source's own search discretization; residuals of ±1–3 % between independent implementations of the same limit-equilibrium method are normal and documented in the sources themselves.

6. Conclusions

Across 61 replicated benchmark cases from two independent published verification suites, now including dry and water-filled tension cracks, a reinforced (micro-pile) slope, non-circular slip surfaces (a predefined weak-seam polyline, two block searches, and a composite circular surface along a weak layer), depth-varying undrained strength, and a linearly-varying (trapezoidal) surcharge, the engine's simplified-Bishop factors of safety agree with published values to a mean of 1.0 % (max 4.7 %, on a benchmark whose published sources themselves span 1.14–1.19; our value matches the original author's to 0.4 %), its Morgenstern–Price implementation agrees with published GLE/Spencer values to a mean of 1.7 %, and 57 of the 59 primary comparisons fall within 5 %. The two exceptions are both search-landscape divergences on the same dipping ACADS weak-layer mechanism. The first is the block-search case #7, a conservative-side divergence corroborated by the GeoStudio variant of the identical problem and refuted as a solver defect by its specified-surface companions. The second is the SLOPE/W §2.9 external-loading case (+6.7 %), whose companion problem, the same mechanism with a piezometric surface and a new trapezoidal surcharge, is reproduced by our block search to +2.1 % against the identical problem's own Slide2 publication (#9); GeoStudio's restriction to a circular search, not an engine defect, explains the larger gap. The one published reinforced circular benchmark, Slide2 #54's stabilising micro-piles, is reproduced to +1.4 %, and the engine's four reinforcement element types (anchor, soil nail, geosynthetic, pile) are demonstrated on a common slope. The campaign is fully scripted and reproducible, and each replicated model is provided as a loadable model input file, available for download.

References

- Arai, K. & Tagyo, K. (1985). *Determination of noncircular slip surface giving the minimum factor of safety in slope stability analysis.* Soils and Foundations, 25(1), 43–51.
- Baker, R. (2003). *Inter-relations between experimental and computational aspects of slope stability analysis.* International Journal for Numerical and Analytical Methods in Geomechanics, 27, 379–401.
- Bishop, A.W. (1955). *The use of the slip circle in the stability analysis of slopes.* Géotechnique, 5(1), 7–17.
- Chen, Z. & Shao, C. (1988). *Evaluation of minimum factor of safety in slope stability analysis.* Canadian Geotechnical Journal, 25(4), 735–748.
- Duncan, J.M. & Wright, S.G. (2005). *Soil Strength and Slope Stability.* John Wiley & Sons.
- Fredlund, D.G. & Krahn, J. (1977). *Comparison of slope stability methods of analysis.* Canadian Geotechnical Journal, 14(3), 429–439.
- GEO-SLOPE International. *Stability Modeling with SLOPE/W: Verification Manual.*
- Giam, S.K. & Donald, I.B. (1989). *Example problems for testing soil slope stability programs.* Civil Engineering Research Report No. 8/1989, Monash University (ACADS).
- Greco, V.R. (1996). *Efficient Monte Carlo technique for locating critical slip surface.* Journal of Geotechnical Engineering, 122(7), 517–525.
- Janbu, N. (1973). *Slope stability computations.* In R.C. Hirschfeld & S.J. Poulos (eds.), Embankment-Dam Engineering, Casagrande Volume, Wiley, 47–86.
- Low, B.K. (1989). *Stability analysis of embankments on soft ground.* Journal of Geotechnical Engineering, 115(2), 211–227.
- Morgenstern, N.R. & Price, V.E. (1965). *The analysis of the stability of general slip surfaces.* Géotechnique, 15(1), 79–93.
- Rocscience Inc. (2022). *Slide2 Slope Stability Verification Manual.*
- Yamagami, T. & Ueta, Y. (1988). *Search for noncircular slip surfaces by the Morgenstern-Price method.* Proceedings of the 6th International Conference on Numerical Methods in Geomechanics, Innsbruck, 1335–1340.

Appendix A: Replicated Slide2 models and results

Each case below is provided as a loadable model input file, available for download, carrying the exact inputs and the published values. Δ (primary) compares our Bishop against the published Bishop where available, otherwise our Morgenstern–Price against the published GLE/Spencer. Literature *Reference* values (sometimes a different mechanism, e.g. planar) are shown for context and never counted as deviations.

Table A1: Model configurations

Case	Description (source)	Materials	Pore pressure	Seismic	Loads	Units	Surface
001	Homogeneous slope, dry (ACADS 1(a)), Slide2 #1	1	dry	—	—	metric	auto-search
002	Homogeneous slope, water-filled tension crack (ACADS 1(b)), Slide2 #2	1	dry	—	—	metric	auto-search + crack
003	Three-layer slope, dry (ACADS 1(c)), Slide2 #3	3	dry	—	—	metric	auto-search
004	Three-layer slope, dry, seismic k_h = 0.15 (ACADS 1(d)), Slide2 #4	3	dry	k_h = 0.15	—	metric	auto-search
005	Talbingo Dam, end of construction (4 materials), Slide2 #5	4	dry	—	—	metric	auto-search
006	Talbingo Dam, 4 materials, predefined circular slip surface (ACADS 2(b)), Slide2 #6	4	dry	—	—	metric	specified circle
007	Slope with thin weak layer, block-searched non-circular surface (ACADS 3(a)), Slide2 #7	2	dry	—	—	metric	block search
008	Slope with thin weak layer, predefined non-circular surface (ACADS 3(b)), Slide2 #8	2	dry	—	—	metric	specified polyline
009	Slope with dipping weak layer, water table, trapezoidal surcharge, block-searched non-circular surface (ACADS 4), Slide2 #9	2	phreatic line	—	surcharge ×2 (1 trapezoidal)	metric	block search
014	Homogeneous slope, dry (Arai and Tagyo example #1), Slide2 #14	1	dry	—	—	metric	auto-search
015	Three-material layered slope with weak middle layer (Arai and Tagyo example 2), Slide2 #15	3	dry	—	—	metric	auto-search
016	Homogeneous slope with water table (Arai and Tagyo example #3), Slide2 #16	1	phreatic line	—	—	metric	auto-search
017	Homogeneous slope, dry (Yamagami & Ueta), Slide2 #17	1	dry	—	—	metric	auto-search
020	Layered slope, 4 materials, weak seam, water table (circular search), Slide2 #20	4	phreatic line	—	—	metric	focused search
021a	Homogeneous slope, dry (Case 1), Slide2 #21	1	dry	—	—	imperial	specified circle

Case	Description (source)	Materials	Pore pressure	Seismic	Loads	Units	Surface
021b	Homogeneous slope, ru = 0.25 pore pressure (Case 2), Slide2 #21	1	r_u = 0.25	—	—	imperial	specified circle
022a	Fredlund & Krahn weak-layer slope, composite surface, dry (Case 1), Slide2 #22	2	dry	—	—	imperial	composite polyline
022b	Fredlund & Krahn weak-layer slope, composite surface, ru = 0.25 (Case 2), Slide2 #22	2	r_u = 0.25	—	—	imperial	composite polyline
023	Three-layer slope, depth-varying undrained c_u 15→30 kN/m^2 (Low 1989), Slide2 #23	3	dry	—	—	metric	specified circle
024	Three-layer undrained slope (Low 1989), Slide2 #24	3	dry	—	—	metric	auto-search
028a	Embankment on soft clay foundation (Example 5), circle tangent to embankment/foundation interface, Slide2 #28	2	dry	—	—	metric	specified circle
028b	Embankment on soft clay foundation (Example 5), circle tangent to base of soft foundation layer, Slide2 #28	2	dry	—	—	metric	specified circle
036	Homogeneous slope with ru pore pressure (deterministic Bishop minimum from probabilistic study), Slide2 #36	1	r_u = 0.2	—	—	metric	auto-search
043	Homogeneous dry slope, critical circular surface in Zone A (Baker planar-comparison problem), Slide2 #43	1	dry	—	—	metric	auto-search
044a	Homogeneous slope, Mohr-Coulomb envelope (Baker example 1, linear fit $c' = 5.3$, $\varphi' = 23$), Slide2 #44	1	dry	—	—	metric	auto-search
044b	Homogeneous slope, Mohr-Coulomb with Baker's iterated parameters ($c' = 0.39$, $\varphi' = 38.6$), Slide2 #44	1	dry	—	—	metric	auto-search
045a	Homogeneous slope (Baker 2003), linear Mohr-Coulomb envelope, Slide2 #45	1	dry	—	—	metric	auto-search
045b	Homogeneous slope (Baker 2003), Mohr-Coulomb from Baker's iterative fit, Slide2 #45	1	dry	—	—	metric	auto-search
052a	Zhu & Lee 4-material slope, dry tension crack, Surface 1, dry, Slide2 #52	4	dry	—	—	metric	specified circle + crack
052b	Zhu & Lee 4-material slope, dry tension crack, Surface 1, wet, Slide2 #52	4	phreatic	—	—	metric	specified circle + crack
052c	Zhu & Lee 4-material slope, dry tension crack, Surface 3, dry, Slide2 #52	4	dry	—	—	metric	specified circle + crack
052d	Zhu & Lee 4-material slope, dry tension crack, Surface 3, wet, Slide2 #52	4	phreatic	—	—	metric	specified circle + crack
054	Homogeneous slope (Yamagami micro-pile problem), unreinforced case, Slide2 #54	1	dry	—	—	metric	auto-search
054r	Homogeneous slope, single micro-pile row (Yamagami micro-pile problem, reinforced), Slide2 #54	1	dry	—	pile ×1	metric	auto-search
061	Homogeneous slope, Mohr-Coulomb criterion (Baker example 3), Slide2 #61	1	dry	—	—	metric	auto-search
062a	Homogeneous slope, dry, pseudo-static seismic k_h = 0.432 (critical seismic coefficient), Slide2 #62	1	dry	k_h = 0.432	—	metric	auto-search

Case	Description (source)	Materials	Pore pressure	Seismic	Loads	Units	Surface
062b	Homogeneous slope, r_u = 0.5, pseudo-static seismic k_h = 0.132 (critical seismic coefficient), Slide2 #62	1	r_u = 0.5	k_h = 0.132	—	metric	auto-search
067	Embankment on foundation, 2 materials, end of construction (USACE F-5), Slide2 #67	2	dry	—	—	imperial	specified circle
074	Sand embankment on saturated clay foundation (2 materials), Slide2 #74	2	dry	—	—	imperial	auto-search
075	James Bay Dyke, 4 materials (circular case), Slide2 #75	4	dry	—	—	metric	auto-search
078a	Pure cohesive slope, 30 ft foundation, slip surface through toe (Case 1a), Slide2 #78	1	dry	—	—	imperial	auto-search
078b	Pure cohesive slope, 30 ft foundation, slip surface tangent to foundation base (Case 1b), Slide2 #78	1	dry	—	—	imperial	specified circle
078c	Pure cohesive slope, 46.5 ft foundation, slip surface through toe (Case 2a), Slide2 #78	1	dry	—	—	imperial	auto-search
078d	Pure cohesive slope, 46.5 ft foundation, slip surface tangent to foundation base (Case 2b), Slide2 #78	1	dry	—	—	imperial	specified circle
078e	Pure cohesive slope, 60 ft foundation, slip surface through toe (Case 3a), Slide2 #78	1	dry	—	—	imperial	auto-search
078f	Pure cohesive slope, 60 ft foundation, slip surface tangent to foundation base (Case 3b), Slide2 #78	1	dry	—	—	imperial	specified circle
079a	Cohesionless embankment on $\varphi = 0$ foundation - Case 1 deep circle tangent to foundation base, Slide2 #79	2	dry	—	—	imperial	auto-search
080a	Embankment on 6-layer stratified foundation, circle tangent to 0 ft depth, Slide2 #80	6	dry	—	—	imperial	specified circle
080b	Embankment on 6-layer stratified foundation, circle tangent to 15 ft depth, Slide2 #80	6	dry	—	—	imperial	specified circle
081a	Two-material embankment - deep circle tangent to foundation base, Slide2 #81	2	dry	—	—	imperial	specified circle
083b	Embankment wall on undrained foundation, constant c_u (Case 2), Slide2 #83	2	dry	—	—	imperial	auto-search
084a	Earth embankment on undrained foundation, profile I ($c_z = 0$), Slide2 #84	2	dry	—	—	imperial	auto-search
102	Homogeneous embankment dam, dry conditions (rapid-drawdown problem, static dry case only), Slide2 #102	1	dry	—	—	metric	auto-search

Table A2: Factor-of-safety comparison

Case	Ours: Bishop	M-P	Janbu (f_0)	Ordinary	Published: Bishop	GLE / Spencer	Janbu corr.	Reference	Δ (primary)
001	0.987	0.986	0.991	0.943	0.987	0.986	0.990	1.000	-0.0%
002	1.588	1.585	1.477	1.516	1.596	1.592	1.489	1.650	-0.5%
003	1.392	1.364	1.349	1.223	1.405	1.374	1.357	1.390	-0.9%
004	1.007	0.981	0.961	0.935	1.016	0.989	0.965	1.000	-0.9%
005	1.966	1.966	1.978	1.957	1.948	1.948	1.949	1.950	+0.9%
006	2.209	2.301	2.085	2.075	2.208	2.301	2.073	2.290	+0.1%
007	—	1.200	1.234	—	1.258	1.275	1.258	—	-5.9%
008	—	1.254	1.283	—	—	1.262	1.294	1.340	-0.6%

Case	Ours: Bishop	M-P	Janbu (f_0)	Ordinary	Published: Bishop	GLE / Spencer	Janbu corr.	Reference	Δ (primary)
009	—	0.735	0.848	—	—	0.720	0.734	0.780	+2.1%
014	1.406	1.410	1.418	1.344	1.409	1.414	1.407	1.451	-0.2%
015	0.414	0.432	0.433	0.415	0.420	0.437	0.423	0.417	-1.4%
016	1.113	1.125	1.097	1.091	1.118	1.118	1.131	1.138	-0.5%
017	1.342	1.344	1.330	1.273	1.344	—	—	1.348	-0.1%
020	1.085	1.095	1.068	1.023	1.087	1.093	—	1.080	-0.1%
021a	2.075	2.075	2.023	1.926	2.079	2.075	—	2.080	-0.2%
021b	1.758	1.765	1.712	1.683	1.763	1.760	—	1.766	-0.3%
022a	—	1.392	1.446	—	1.382	1.372	—	—	+1.4%
022b	—	1.139	1.180	—	1.124	1.114	—	—	+2.3%
023	1.136	1.301	1.629	1.326	1.192	—	—	—	-4.7%
024	1.438	1.438	1.566	1.438	1.439	—	—	1.440	-0.1%
028a	1.158	1.158	1.162	1.116	1.160	—	—	1.163	-0.1%
028b	1.177	1.175	1.123	1.135	1.185	—	—	1.148	-0.7%
036	1.335	1.355	1.343	1.370	1.340	—	—	1.334	-0.3%
043	1.242	1.353	1.378	1.298	—	—	—	1.350	—
044a	0.996	0.998	1.003	0.950	—	1.536	—	1.500	n/a †
044b	0.970	0.971	0.984	0.952	—	0.981	—	0.970	-1.0%
045a	2.835	2.834	2.834	2.709	—	2.794	—	2.660	+1.4%
045b	2.681	2.680	2.718	2.621	—	2.696	—	2.640	-0.6%
052a	2.008	2.015	1.982	1.931	2.010	2.017	—	2.035	-0.1%
052b	1.524	1.532	1.528	1.513	1.526	1.533	—	1.560	-0.1%
052c	1.775	1.761	1.721	1.495	1.804	1.790	—	1.744	-1.6%
052d	1.154	1.152	1.147	1.028	1.176	1.174	—	1.166	-1.9%
054	1.101	1.102	1.089	1.041	1.102	—	—	1.100	-0.1%
054r	1.209	1.208	1.171	1.132	1.193	—	—	1.200	+1.4%
061	1.315	1.318	1.330	1.256	—	1.366	—	1.350	-3.5%
062a	0.992	1.002	0.983	1.041	0.991	1.001	—	1.000	+0.1%
062b	0.987	1.006	0.961	1.026	0.987	1.001	—	1.000	+0.0%
067	1.324	1.321	1.346	1.303	1.332	1.327	1.345	1.330	-0.6%
074	1.190	1.177	1.125	1.042	1.228	1.201	1.174	1.220	-3.1%
075	1.517	1.517	1.529	1.366	1.468	1.466	—	1.450	+3.3%
078a	1.109	1.109	1.245	1.109	1.126	1.186	—	1.124	-1.5%
078b	1.133	1.133	1.264	1.133	1.141	1.139	—	—	-0.7%
078c	1.106	1.106	1.220	1.106	1.126	1.186	—	1.124	-1.8%
078d	1.121	1.121	1.232	1.121	1.130	1.129	—	1.124	-0.8%
078e	1.106	1.106	1.212	1.106	1.125	1.185	—	1.124	-1.7%
078f	1.114	1.114	1.224	1.114	1.125	1.124	—	1.119	-1.0%
079a	1.398	1.395	1.338	1.308	1.412	1.404	—	1.400	-1.0%
080a	2.525	2.524	2.371	2.210	2.549	2.550	—	2.560	-0.9%
080b	1.420	1.377	1.389	1.253	1.398	1.358	—	1.350	+1.6%
081a	1.221	1.211	1.165	1.106	1.230	1.217	—	1.210	-0.8%
083b	1.337	1.335	1.297	1.255	1.335	1.331	—	1.312	+0.1%
084a	0.739	0.737	0.707	0.686	0.761	0.762	—	0.750	-2.9%
102	2.506	2.504	2.517	2.400	—	2.455	—	2.430	+2.0%

† #44a's published Mohr-Coulomb values are internally inconsistent with the manual's own stated geometry and properties (see §4.3); the case is reported without a deviation statistic.